Dynamics of the helium atom close to the full fragmentation threshold: Ionization excitation

C. Bouri,* P. Selles, and L. Malegat
Laboratoire d'Interaction du rayonnement X Avec la Matière (Laboratoire associé au CNRS), Université Paris-Sud, 91405 Orsay, France

J. M. Teuler
Laboratoire de Chimie Physique (Laboratoire associé au CNRS), Université Paris-Sud, 91405 Orsay, France

M. Kwato Njock
CEPAMOQ, University of Douala, Douala, Cameroon

A. K. Kazansky
Fock Institute of Physics, University of St. Petersburg, 198504, Russia
(Received 7 June 2005; published 27 October 2005)

The hyperspherical $\mathcal{R}$-matrix method with semiclassical outgoing waves, designed to provide accurate double-ionization cross sections, is extended to allow for the computation of ionization-excitation data of comparable quality. Accordingly, it appears now as a complete method for treating the correlated dynamics of two-electron atoms, in particular above their full fragmentation threshold. Cross sections σ_n and asymmetry parameters β_n are obtained for single photoionization of helium with excitation of the residual ion up to as high a level as $n=50$ at 0.1 eV above the double-ionization threshold. These data are extrapolated to infinite values of n in order to check widespread assumptions regarding this limit. Our data are found consistent with the assumed n^{-3} dependence of the partial ionization cross sections. However, the $\beta_\infty=-0.636$ obtained still lies far from the -1 value expected at the double-ionization threshold.

DOI: 10.1103/PhysRevA.72.042716 PACS number(s): 32.80.Fb

I. INTRODUCTION

Describing the double-electronic continuum that arises from such fundamental processes as electron impact ionization of H or double photoionization of He has remained a challenge for computational atomic physics until very recently. It is only in the last few years that methods have appeared which deal with this problem quantitatively (see [1] for the results up to 2000 and [2] for more recent work). As a result, it is now possible to compute electron impact ionization cross sections of H and double-photoionization cross sections of He which reproduce absolute measurements within the experimental uncertainty. However, full control of the intricate dynamics initiated by electron impact on H above the single-ionization threshold or by photon impact on He above the double-ionization threshold will not be demonstrated until one masters the resulting distribution of the outgoing flux between all members of the infinite set of available exit channels. For electron impact on H, this means that one should be able to disentangle precisely the elastic scattering channel $e+H_{n=1}$, the ionization channel $e+e+H^+$, and the infinite series of excitation channels $e+H_{n=2\cdots\infty}$. Similarly, for photon impact on He, one should separate the single-ionization channel $e+He_{n=1}^+$, the double-ionization channel $e+e+He^{2+}$, and the infinite series of single-ionization channels with excitation of the residual ion $e+He_{n=2\cdots\infty}^+$ accurately. Accordingly, one should be capable of checking numerically the continuity between excitation to high-lying bound states and excitation to the continuum which is expected at threshold. However, to the best of our knowledge, this program has not been completed yet. It was brought to our attention after submission of this paper that this program has been completed in the limit of very high photon energies [25]. This is why we have set out to fill this gap. The present paper reports on our first progress in this direction. It shows that the hyperspherical $\mathcal{R}$-matrix method with semiclassical outgoing waves (H$\mathcal{R}$SOW), which has provided accurate double-ionization cross sections, can be complemented to yield single-ionization data as well. Interestingly, the method yields cross sections for single ionization with excitation up to levels as high as $n=50$, which have not been considered in the numerous previous calculations based on standard close-coupling and $\mathcal{R}$-matrix techniques and on their various sucessful avatars including convergent-close-coupling (CCC), hyperspherical-close-coupling (HSCC), eigenchannel $\mathcal{R}$-matrix, or $\mathcal{R}$-matrix with pseudostates methods. The data obtained can then be extrapolated to $n=\infty$. Section II recalls the hyper-radial propagation scheme inherent to the method and presents recent improvements of its numerical implementation. Section III demonstrates the fixed hyper-radius projection technique used to separate the various single-ionization channels from each other and from the double-ionization one in the course of propagation. Section IV presents cross sections and asymmetry parameters for ionization excitation up to $n=50$ at 0.1 eV above the double-ionization threshold. It reports our

*Permanent address: CEPAMOQ, University of Douala, Douala, Cameroon.

attempts at extrapolating these data to $n=\infty$. The concluding Sec. V announces further developments.

II. HYPER-RADIAL PROPAGATION

A. General framework

The H$\mathcal{R}$MSOW method proposes a simple scheme to compute the wave function of a helium atom, initially in its ground state $\Psi_0(\vec{r}_1,\vec{r}_2)$ of energy E_0, after it has absorbed a single photon carrying an energy larger than the He double-ionization potential. This photoionization wave function, denoted $\bar{\Psi}(\vec{r}_1,\vec{r}_2)$, is obtained by solving the stationary inhomogeneous Schrödinger equation

$$[H-(E_0+\omega)]\bar{\Psi}(\vec{r}_1,\vec{r}_2)=-\frac{1}{2}\vec{\mathcal{E}}\cdot\vec{D}\Psi_0(\vec{r}_1,\vec{r}_2) \tag{1}$$

for an outgoing-wave asymptotic condition. In Eq. (1), H denotes the field-free two-electron Hamiltonian, and $\vec{D}$ the dipole operator that couples the atom to the external electric field of amplitude $\vec{\mathcal{E}}$ and frequency ω. This equation is solved in a set of partially collective coordinates which consists of the hyperspherical radius $R=\sqrt{r_1^2+r_2^2}$, the radial correlation angle $\alpha=\tan^{-1}(r_2/r_1)$, and the spherical angles θ_1,φ_1, and θ_2,φ_2, that specify the directions of the unit vectors $\hat{r}_1$ and $\hat{r}_2$. For convenience, we introduce the compact notations $\Omega_1=\{\theta_1,\varphi_1\}$, $\Omega_2=\{\theta_2,\varphi_2\}$, and $\Omega=\{\alpha,\Omega_1,\Omega_2\}$. The R^{-1} dependence of the three-body Coulomb potential

$$C(R,\alpha,\theta_{12})=-\frac{1}{R}\left(\frac{Z}{\cos\alpha}+\frac{Z}{\sin\alpha}-\frac{1}{\sqrt{1-\sin 2\alpha\cos\theta_{12}}}\right)$$
$$=-\frac{Z_{eff}(\alpha,\theta_{12})}{R}, \tag{2}$$

where $\theta_{12}=\cos^{-1}(\hat{r}_1\cdot\hat{r}_2)$ and $Z=2$, suggests separating configuration space into two regions: an inner region $R\leqslant R_0$ where the R dependence is strong, and a complementary outer region where it is weak enough to support a semiclassical treatment. The inner-region calculation provides the solution $\bar{\Psi}(R_0;\Omega)$ on the hypersphere $R=R_0$. It does so by expressing both the $\mathcal{R}$-matrix condition derived from Eq. (1) and the outgoing-wave asymptotic condition at $R=R_0$ within the adiabatic angular basis defined on this hypersphere. The details of this inner-region treatment can be found in [3–5] and do not matter here. By contrast, the outer-region treatment is highly relevant to our present purpose. We recall its main features below in more detail than in previous publications.

B. Approximations

The outer-region treatment consists in neglecting the short-range right-hand side of Eq. (1) and in looking for the solution in the form

$$\bar{\Psi}(R;\Omega)=\frac{1}{R^{5/2}\sin 2\alpha}\frac{1}{\sqrt{p(R,E)}}$$
$$\times\exp\left(\imath\int_{R_0}^{R}p(R',E)dR'\right)\bar{\Phi}(R;\Omega), \tag{3}$$

where $E=E_0+\omega$ denotes the total energy of the system. The first term, related to the volume element in the current coordinates, is introduced for computational convenience and does not imply any approximation. The second term is the semiclassical outgoing wave (SOW) that is outlined in the very name of the method. The last term is a reduced function that is supposed to depend only weakly on R. In writing Eq. (3), one is making two assumptions: (i) that the bulk of the hyper-radial (R) motion can be separated from the angular (Ω) motion to a reasonable extent, and (ii) that this motion can be described by a *unique, semiclassical, outgoing* wave associated with a local momentum $p(R,E)$ that remains to be specified.

The idea behind assumption (i) is that R, which measures the overall size of the electron-ion-electron triangle, is less critical to the dynamics than the angular parameters α and θ_{12} that control the shape of this triangle. This idea, which will be supported by the success of the resulting approach, can hardly be justified *a priori* by the quantitative estimate of any relevant quantity. Practically, it implies that the energy and momentum associated with the R dependence of the reduced function $\bar{\Phi}$ are negligible with respect to their counterparts arising from the SOW, which can be expressed by the two conditions

$$\frac{\partial^2\bar{\Phi}}{\partial R^2}\ll p^2\bar{\Phi},\quad \frac{\partial\bar{\Phi}}{\partial R}\ll p\bar{\Phi}. \tag{4}$$

To figure out what the bulk of the R motion looks like, let us consider more carefully the three-body potential of Eq. (2) that determines this motion. At fixed $R\geqslant R_0$, $C(R,\alpha,\theta_{12})$ has the well-known shape of a saddle: two infinite barriers at $(\alpha=\pi/4,\theta_{12}=0)$ and $(\alpha=\pi/4,\theta_{12}=2\pi)$ and two infinite wells at $(\theta_{12}=\pi,\alpha=0)$ and $(\theta_{12}=\pi,\alpha=\pi/2)$ break through the large plateau that extends around the saddle point $(\alpha=\pi/4,\theta_{12}=\pi)$. Paying tribute to the work of Wannier, we denote by Z_W the saddle-point effective charge, which determines the level of the plateau. The barriers, which define *forbidden* areas, have no influence on the definition of an effective local momentum. The wells, by contrast, play an important role which can nevertheless be reduced drastically by a proper redefinition of the outer region function. Figure 1 suggests the proper scheme in the illustrative case where $R=R_0=25$ a.u. It shows that the lowest three hydrogenic levels E_n of the He^+ ion are located below the top of the potential barrier. Accordingly, each of these levels is associated with two separate classically allowed intervals of width $\Delta\alpha_n$ located around $\alpha=0$ and $\pi/2$, respectively. In addition, for $n=1$ and 2, $R_0\Delta\alpha_n$ turns out to be very close to the range r_n of the nth hydrogenic level. This means that single ionization leaving the residual ion in the levels 1 and 2 can be properly described at $R_0=25$ a.u. In other words, the two-electron wave function of energy $E>0$ extracted at this distance has

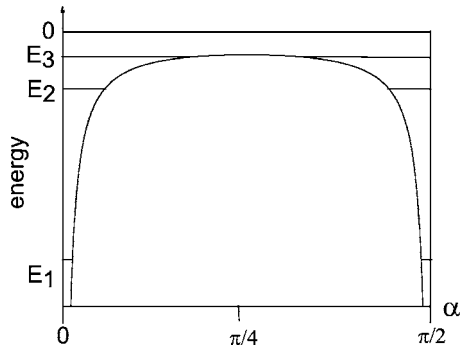

FIG. 1. Qualitative cut of the three-body Coulomb potential $C(R,\alpha,\theta_{12})$ along α at $\theta_{12}=\pi$ rad and $R_0=25$ u.a. The horizontal segments depict the α-intervals which are classically allowed at the energies $E_n=-Z^2/2n^2$ of the $n=1$ to 3 levels of He^+ which lie below the top of the barrier at $-Z_W/R_0$.

components, confined within $\Delta\alpha_n$ sectors about $\alpha=0$ and $\pi/2$, which can be associated with single ionization leaving the residual ion in the level n—the photoelectron taking away the excess energy $E-E_n$. The simplest way to disentangle these components from the bulk of the wave function is to expand the latter over the "locally adapted" angular basis vectors (also referred to as "adiabatic" angular basis vectors) which diagonalize the Hamiltonian at fixed $R=R_0$. We have shown indeed in previous publications that the groups of adiabatic channels {1}, {2–4}, {5–9} defined at $R_0 \geqslant 50$, for instance, could be associated with ionization excitation to the levels 1, 2, and 3, respectively, the multiplicity of each group of adiabatic channels being equal to the first-order Stark degeneracy of each hydrogenic level. This possibility of disentangling the lowest single-ionization channels from the rest of the wave function at R_0 is the key that makes assumption (ii) work. From the total wave function $\bar{\Psi}(R_0;\Omega)$ derived from the inner region, let us indeed subtract the single-ionization channels $n=1,\ldots,n_{R_0}$ that can be identified at R_0, thus defining a new function $\tilde{\Psi}(R_0;\Omega)$. This simple operation amounts to filling the wells in Fig. 1 up to the level $E_{n_{R_0}}$. The effective potential experienced by the new function then reduces approximately to a flat surface at $-Z_W/R$. From the latter, a unique local momentum

$$p(R,E)=\sqrt{2\left(E+\frac{Z_W}{R}\right)} \tag{5}$$

can be defined. The condition that guarantees the validity of the semiclassical approximation can then be written in terms of the local wavelength $\lambda(R,E)=p^{-1}(R,E)$ as

$$\lambda_R'(R,E) \ll 1. \tag{6}$$

Figure 2 shows that Eq. (6) is satisfied within a wide energy × hyper-radius domain. In particular, very-low-energy calculations can be accommodated within inner regions of manageable sizes. As the outgoing-wave boundary condition has already been imposed at R_0 by the inner-region treatment, we do not introduce any additional approximation when we assume an outgoing-wave behavior for the outer-region wave function. As a result, we can state that the new

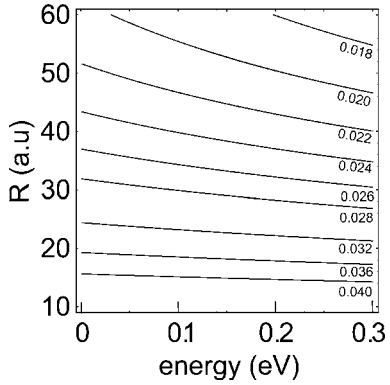

FIG. 2. Contour lines of $\lambda_R'(R,E)$.

function Ψ, cleared of all single-ionization channels that can be identified at R_0, will be described reasonably well by a unique SOW of the form given in Eq. (3) with the momentum given by Eq. (5).

C. Propagators

Details regarding the subtraction of the single-ionization channels at R_0, as well as the definition of a more refined expression of the charge that enters the local momentum $p(R,E)$ can be found in previous publications, notably in [6]. It is sufficient for our present purpose to state that we are now left with a new wave function $\Psi(R;\Omega)$, which is known at R_0 from the inner-region calculation, which depends on a new reduced wave function $\Phi(R;\Omega)$ according to Eq. (3), and which satisfies the homogeneous counterpart of Eq. (1) for $R \geqslant R_0$. The approximation expressed by Eq. (4) implies that the second-order partial derivative of Φ with respect to R can be neglected. This reduced wave function then satisfies a partial differential equation of first order in R that can be rewritten in the standard form of a propagation equation if one shifts from the variable R to the new variable τ such that $Rp(R,E)d\tau=dR$. One gets

$$\imath\frac{\partial}{\partial\tau}\Phi(\tau;\Omega)=\mathcal{H}\Phi(\tau;\Omega), \tag{7}$$

where $\mathcal{H}$ is obtained from H by (i) neglecting the second-order derivative with respect to R, (ii) suppressing the terms that depend only on R, since they would contribute to the R evolution only through an overall irrelevant phase factor, and (iii) multiplying the resulting expression by R.

Introducing an appropriate representation of Φ reveals the different properties of the various terms in $\mathcal{H}$. Assuming linear polarization along the z axis makes Φ a ${}^1P^o_{M=0}$ wave function which is conveniently expanded on orthonormal symmetrized bipolar harmonics ${}^{\epsilon}\mathcal{Y}^{10}_{\ell\ell+1}(\Omega_1,\Omega_2)$ according to

$$\Phi(\tau;\alpha,\Omega_1,\Omega_2)=\sum_{\ell=0}^{n_\ell-1}\sum_{\epsilon=\pm1}a_\ell^{\epsilon}(\tau;\alpha)\,{}^{\epsilon}\mathcal{Y}^{10}_{\ell\ell+1}(\Omega_1,\Omega_2), \tag{8}$$

where $\epsilon=+1$ indicates symmetry in the exchange of the two electrons and $\epsilon=-1$ antisymmetry. Inserting this expansion into Eq. (7) yields the following set of coupled partial differential equations for the coefficients $a_\ell^{\epsilon}(\tau;\alpha)$:

$$\iota\frac{\partial}{\partial\tau}a_\ell^\epsilon(\tau;\alpha)=\left(-\frac{1}{2R(\tau)}\frac{\partial^2}{\partial\alpha^2}+\mathcal{U}_\ell(\tau;\alpha)\right)a_\ell^\epsilon(\tau;\alpha)+\mathcal{V}_\ell(\tau;\alpha)a_\ell^{-\epsilon}(\tau;\alpha)+\sum_{\ell'}\mathcal{W}_{\ell\ell'}^\epsilon(\alpha)a_{\ell'}^\epsilon(\tau;\alpha), \tag{9}$$

where

$$\mathcal{U}_\ell(\tau;\alpha)=\frac{2(\ell+1)^2}{R(\tau)\sin^2 2\alpha}-\frac{Z}{\cos\alpha}-\frac{Z}{\sin\alpha},$$
$$\mathcal{V}_\ell(\tau;\alpha)=\frac{2(\ell+1)\cos 2\alpha}{R(\tau)\sin^2 2\alpha}, \tag{10}$$

and

$$\mathcal{W}_{\ell\ell'}^\epsilon(\alpha)=\langle {}^\epsilon\mathcal{Y}_{\ell\ell+1}^{10}|\mathcal{W}|{}^\epsilon\mathcal{Y}_{\ell'\ell'+1}^{10}\rangle_{\Omega_1,\Omega_2}$$
$$\text{where } \mathcal{W}=R/r_{12}=\frac{1}{\sqrt{1-\sin 2\alpha\cos\theta_{12}}}, \tag{11}$$

integration over the two solid angles Ω_1 and Ω_2 being assumed in the first of Eqs. (11). Equation (9) shows two groups of terms with contrasted properties. $\mathcal{W}_{\ell\ell'}^\epsilon(\alpha)$, on one hand, does not depend on τ, shows no singularity in α, and couples far-distant partial waves ℓ and ℓ' at given ϵ and α. On the other hand, the remaining terms depend on τ, $\mathcal{U}_\ell(\tau;\alpha)$, and $\mathcal{V}_\ell(\tau;\alpha)$, show singularities at $\alpha=0$ and $\pi/2$, and $\mathcal{V}_\ell(\tau;\alpha)$ connects symmetric and antisymmetric components at given ℓ and α while the differential operator couples neighboring values of α at given ℓ and ϵ. It would then be convenient to consider the respective contributions of these two groups of terms to the propagation process separately.

The split-operator method [7] meets this need. It allows one to write the elementary propagator over $d\tau$ under the influence of $\mathcal{H}=A+B$ as

$$P(d\tau;A+B)=P(d\tau/2;A)P(d\tau;B)P(d\tau/2;A) \tag{12}$$

within third order in $d\tau$, so that the propagator over $\tau=n\,d\tau$ reads

$$P(\tau;A+B)=P(d\tau/2;A)[P(d\tau;B)P(d\tau;A)]^nP(-d\tau/2;A). \tag{13}$$

It is clear from Eq. (13) that A and B contribute on an equal footing to the core of the propagation that is represented by the central square brackets. Let us then take $A=\mathcal{W}$ and $B=\mathcal{H}-A$—it being understood that the opposite choice would be essentially equivalent.

The evolution controlled by A obeys

$$\iota\frac{\partial}{\partial\tau}a_\ell^\epsilon(\tau;\alpha)=\sum_{\ell'}\mathcal{W}_{\ell\ell'}^\epsilon(\alpha)a_{\ell'}^\epsilon(\tau;\alpha), \tag{14}$$

whereas that controlled by B is expressed more simply in terms of the alternative coefficients

$$b_\ell^\pm(\tau;\alpha)=\frac{1}{\sqrt{2}}[a_\ell^+(\tau;\alpha)\pm a_\ell^-(\tau;\alpha)], \tag{15}$$

which satisfy the following set of partial differential equations:

$$\iota\frac{\partial}{\partial\tau}b_\ell^\mu(\tau;\alpha)=\left(-\frac{1}{2R(\tau)}\frac{\partial^2}{\partial\alpha^2}+\mathcal{B}_\ell^\mu(\tau;\alpha)\right)b_\ell^\mu(\tau;\alpha)$$
$$\text{where } \mathcal{B}_\ell^\mu(\tau;\alpha)=\mathcal{U}_\ell(\tau;\alpha)+\mu\mathcal{V}_\ell(\tau;\alpha) \tag{16}$$

with μ taking the values ±1.

Before considering the resolving schemes appropriate to these two equations, we need to complete our representation of the five-dimensional configuration space Ω. As regards α, it is convenient to use a nonuniform grid with a high density of points in the vicinity of the singularities of the three-body potential. Here we take

$$\alpha_i=\left(x_i-\frac{1}{4}\sin 4x_i\right),\quad x_i=\frac{i\pi}{2(n_\alpha+1)},\quad i=1,\ldots,n_\alpha, \tag{17}$$

which ensures an n_α^{-3} step size in the neighborhood of $\alpha=0$ and $\pi/2$. The local potentials in Eqs. (14) and (16) are then represented by their values at the grid points $\mathcal{W}_{\ell\ell'}^\epsilon(\alpha_i)$ and $\mathcal{B}_\ell^\mu(\tau;\alpha_i)$ and the differential operator in Eq. (16) by a second-order difference formula that reads $y_i''=s_iy_{i-1}+c_iy_i+d_iy_{i+1}$, the differentiation weights associated with the nonuniform grid being given by

$$s_i=\frac{2}{(\alpha_{i-1}-\alpha_i)(\alpha_{i-1}-\alpha_{i+1})},\quad c_i=\frac{2}{(\alpha_i-\alpha_{i-1})(\alpha_i-\alpha_{i+1})},$$
$$d_i=\frac{2}{(\alpha_{i+1}-\alpha_{i-1})(\alpha_{i+1}-\alpha_i)}. \tag{18}$$

The propagation equations (14) and (16) can be rewritten in matrix form as

$$\iota\frac{\partial}{\partial\tau}\boldsymbol{a}(\tau)=\boldsymbol{A}\boldsymbol{a}(\tau), \tag{19}$$

$$\iota\frac{\partial}{\partial\tau}\boldsymbol{b}(\tau)=\boldsymbol{B}(\tau)\boldsymbol{b}(\tau), \tag{20}$$

the matrix elements in the relevant N-dimensional representations labeled $(\ell\epsilon i)$ and $(\ell\mu i)$ being given by

$$_{\ell\epsilon i}A_{\ell'\epsilon'i'}=\delta_{\epsilon\epsilon'}\delta_{ii'}\mathcal{W}_{\ell\ell'}^\epsilon(\alpha_i), \tag{21}$$

$$_{\ell\mu i}B_{\ell'\mu'i'}(\tau)=-\delta_{\mu\mu'}\delta_{\ell\ell'}\left[\frac{s_i}{2R(\tau)}\delta_{i,i'+1}+\left(\frac{c_i}{2R(\tau)}-\mathcal{B}_\ell^\mu(\tau;\alpha_i)\right)\delta_{ii'}+\frac{d_i}{2R(\tau)}\delta_{i,i'-1}\right] \tag{22}$$

with $N=2n_\ell n_\alpha$. Equations (21) and (22) evidence the contrasted properties of the two propagation equations (19) and (20) already noted: the τ-independent operator A induces

"long-range" couplings in ℓ, whereas the τ-dependent operator B induces "short-range," namely, tridiagonal, couplings in i. Accordingly, different resolution schemes are applied to these two equations.

With Eq. (19), we associate the elementary propagator

$$P(d\tau;A) = \exp(-\imath\, d\tau A). \tag{23}$$

We take as its matrix representation the exponential of the matrix representation of $-\imath\, d\tau \boldsymbol{A}$, defined as a series expansion in powers of $-\imath\, d\tau \boldsymbol{A}$, which preserves unitarity to all orders in $d\tau$. As A is free of singularities and independent of τ, this computation can be performed safely once for all before propagation starts. As a result, the only task that has to be performed repeatedly to ensure the A part of the propagation is the N-dimensional matrix $\times$ vector multiplication

$$\boldsymbol{a}(\tau + d\tau) = \boldsymbol{P}(d\tau;A)\boldsymbol{a}(\tau). \tag{24}$$

Due to the block-diagonal structure of the matrix $\boldsymbol{A}$, which is conserved in $\boldsymbol{P}(d\tau;A)$, the latter reduces to $2n_\alpha$ independent n_ℓ-dimensional matrix $\times$ vector multiplications.

The above technique is not recommended for the B part of the propagation. Indeed, as B depends on τ, $-\imath\, d\tau \mathbf{B}$ should be exponentiated at each step. This would be a rather heavy task that in addition could fail due to the singularities in B. It is by far more convenient to use an elementary propagator of the Crank-Nicholson form

$$P(d\tau;B) = \left(1 + \imath\frac{d\tau}{2}B\right)^{-1}\left(1 - \imath\frac{d\tau}{2}B\right) \tag{25}$$

since the latter is unitary to all orders in $d\tau$ and allows one to take the best advantage of the particular structure of the matrix $\boldsymbol{B}$, which is not only diagonal by blocks but also tridiagonal within each block. Performing an elementary propagation step thus amounts to solving the N-dimensional inhomogeneous linear system

$$\left(\mathbf{1} + \imath\frac{d\tau}{2}\boldsymbol{B}\right)\boldsymbol{b}(\tau + d\tau) = \left(\mathbf{1} - \imath\frac{d\tau}{2}\boldsymbol{B}\right)\boldsymbol{b}(\tau), \tag{26}$$

which reduces to a set of $2n_\ell$ independent n_α-dimensional tridiagonal systems.

D. Numerical implementation

The elementary propagation step described by the propagator $P(d\tau;B)P(d\tau;A)$ requires one to accomplish (i) $2n_\alpha$ independent n_ℓ-dimensional matrix $\times$ vector multiplications to propagate $\boldsymbol{a}$, (ii) $2n_\ell n_\alpha$ independent two-dimensional linear combinations to pass from $\boldsymbol{a}$ to $\boldsymbol{b}$, (iii) $2n_\ell$ independent solvings of an n_α-dimensional tridiagonal system to propagate $\boldsymbol{b}$, and (iv) $2n_\ell n_\alpha$ independent two-dimensional linear combinations to come back from $\boldsymbol{b}$ to $\boldsymbol{a}$, n_ℓ being of the order of a few tens and n_α of a few thousands. Independent operations appear at each stage but for different fixed labels: $\epsilon\alpha$ at (i), $\mu\ell\alpha$ at (ii), $\mu\ell$ at (iii), $\epsilon\ell\alpha$ at (iv). Any parallelization procedure will therefore require communications between succesive propagation steps, which will reduce its performance, the more so the larger the number of processors invoked. As a result, the problem is no good candidate for massive parallelization, although its resolution could benefit from a moderate parallelization. This is why we have chosen to parallelize on ℓ, which has a reduced range of variation, and to vectorize on α. The vector $\times$ matrix multiplication at stage (i), as well as the linear combinations at stages (ii) and (iv), are obviously highly vectorizable operations, but this is not so for the resolution of the tridiagonal system at stage (iii). However, we have implemented a cyclic reduction algorithm that allows vectorization within each reduction step. See for instance [8] in which it is also called *recursive doubling*. Here, we only wish to point out the interesting performances we obtain this way on the moderately parallel vector computer at IDRIS. Typically, we are able to perform about 90 000 propagation steps for a 50-partial-wave wave function discretized on a 4000-point α grid within 2 h 50 min monoprocessor time. This corresponds to propagating from $R_0 = 60$ to 10^6 a.u. at 0.1 eV above the double-ionization threshold. This increased efficiency of the outer-region propagation is crucial for investigating the progressive decoupling of the increasingly excited single-ionization channels in the course of the R expansion of the system, a subject that is dealt with in the following section.

III. FIXED HYPER-RADIUS PROJECTION

A. Purpose

Until recently, the H$\mathcal{R}$MSOW method had produced only very few single-ionization data, namely, integrated cross sections for single ionization leaving the residual ion in the three lowest hydrogenic levels $n = 1-3$. These were extracted on the hypersphere $R = R_0$ that limits the inner region by identifying the corresponding single-ionization channels with sets of adiabatic channels defined on this hypersphere as noted in Sec. II B. A reduced function, cleared of these few single-ionization channels, was further propagated throughout the outer region till R_{max}. The analysis of the wave function at R_{max} was only qualitative. It was based on the fact that as $R \to \infty$, single ionization corresponding to r_2 finite and r_1 infinite or the opposite becomes confined within vanishingly small α sectors about $\alpha = 0$ and $\pi/2$, whereas double ionization, corresponding to both r_1 and r_2 infinite, is described by the complementary α values in the open interval $]0, \pi/2[$. These values are then related to the sharing of the excess energy between the two electrons since $\alpha \simeq \tan^{-1}\sqrt{E_2/E_1}$. No attempt was made to analyze the final wave function in terms of the various single-ionization channels, which were considered as a whole. As a result, the H$\mathcal{R}$MSOW method did not appear as a complete method for studying the above-the-double-ionization-threshold dynamics of the model three-body system He.

A first attempt to fill this gap was presented in [9]. It was based on projecting the photoionization wave function on the successive hydrogenic levels n of the He^+ ion at appropriate distances R_n. It demonstrated the feasibility of this approach, which is presented in more detail below.

B. Method

In the following, we will label the two electrons of the system by i and $\bar{i}$, respectively, with $\bar{i} = 2$ if $i = 1$ and $\bar{i} = 1$ if

$i=2$. Let us then denote by $|n\ell m;i\rangle$ the hydrogenic eigenstate $n\ell m$ of electron i in the He^{2+} core. It is given in the position representation by

$$\langle \vec{r}|n\ell m;i\rangle = F_{n\ell}(r_i)Y_{\ell m}(\Omega_i), \tag{27}$$

where $Y_{\ell m}$ stands for a normalized spherical harmonic and $F_{n\ell}$ for the normalized radial function

$$F_{n\ell}(r) = \frac{2Z^{3/2}}{n^2}\sqrt{\frac{(n-\ell-1)!}{(n+\ell)!}}\exp\left(\frac{-Zr}{n}\right) \times\left(\frac{2Zr}{n}\right)^{\ell} L_{n-\ell-1}^{2\ell+1}\left(\frac{2Zr}{n}\right), \tag{28}$$

the Laguerre polynomials L_p^q being defined according to the conventions of Abramowitz and Stegun [10]. The projector $|n\ell m;i\rangle\langle n\ell m;i|$ onto this state is termed $P_{n\ell m}^i$. The projected wave function $\Psi_{nlm}^i = P_{n\ell m}^i\Psi$ describes an ionization-excitation process in which electron i is excited to the state $n\ell m$ whereas electron $\bar{i}$ is ejected. The corresponding fully integrated cross section $\sigma_{n\ell m}^i$ follows as the total outgoing flux of $\Psi_{n\ell m}^i$ through a hypersphere $R=R_n$ of adequately large hyper-radius divided by the incoming photon flux. It can be expressed in terms of the reduced wave function $\Phi_{n\ell m}^i$ associated with $\Psi_{n\ell m}^i$ according to Eq. (3) by

$$\sigma_{n\ell m}^i = \frac{2\pi\omega}{c}\int_{R=R_n} d\alpha\, d\Omega_i d\Omega_{\bar{i}}|\Phi_{n\ell m}^i(\alpha,\Omega_i,\Omega_{\bar{i}})|^2. \tag{29}$$

The corresponding differential cross section can be written similarly in terms of the outgoing flux through the elementary surface defined on the hypersphere $R=R_n$ by the solid angle $d\Omega$ centered on Ω as

$$\frac{d\sigma_{n\ell m}^i}{d\Omega} = \frac{2\pi\omega}{c}\int_{R=R_n} d\alpha\, d\Omega_i|\Phi_{n\ell m}^i(\alpha,\Omega_i,\Omega_{\bar{i}}=\Omega)|^2. \tag{30}$$

[Note that, here, $\Omega=(\theta,\varphi)$ denotes the current direction of the photoelectron, and not, as in Sec. II, the set of five angles $(\alpha,\Omega_1,\Omega_2)$.] The fully integrated and differential cross sections for ionization excitation leaving the residual ion in the level n follow from

$$\sigma_n = \sum_{\ell mi}\sigma_{n\ell m}^i \tag{31}$$

and

$$\frac{d\sigma_n}{d\Omega} = \sum_{\ell mi}\frac{d\sigma_{n\ell m}^i}{d\Omega}. \tag{32}$$

The asymmetry parameter β_n, defined by

$$\frac{d\sigma_n}{d\Omega} = \frac{\sigma_n}{4\pi}[1+\beta_n P_2(\cos\theta)], \tag{33}$$

where P_2 stands for the second-order Legendre polynomial, can then be expressed from Eqs. (29)–(33) as

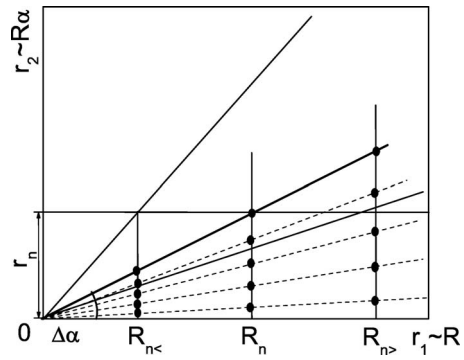

FIG. 3. Accuracy of the fixed-R projection method for a given level n as R increases. (The width of the allowed angular sector has been magnified for clarity.)

$$\beta_n = \sqrt{20\pi}\frac{\sum_{\ell mi}\int_{R=R_n} d\alpha\, d\Omega_i d\Omega_{\bar{i}}|\Phi_{n\ell m}^i|^2 Y_{20}^*(\Omega_{\bar{i}})}{\sum_{\ell mi}\int_{R=R_n} d\alpha\, d\Omega_i d\Omega_{\bar{i}}|\Phi_{n\ell m}^i|^2}. \tag{34}$$

It is worth noting that one can rewrite σ_n and β_n in terms of the reduced wave function Φ_n associated with the projected wave function $\Psi_n=\Sigma_{\ell mi}\Psi_{n\ell m}^i$ which describes single ionization with excitation to the level n; namely

$$\sigma_n = \frac{2\pi\omega}{c}\int_{R=R_n} d\alpha\, d\Omega_1 d\Omega_2|\Phi_n|^2 \tag{35}$$

and

$$\beta_n = \sqrt{20\pi}\frac{\oint_{R=R_n} d\alpha\, d\Omega_1 d\Omega_2|\Phi_n|^2 Y_{20}^*(\Omega_1)}{\oint_{R=R_n} d\alpha\, d\Omega_1 d\Omega_2|\Phi_n|^2}, \tag{36}$$

where the symbol $\oint$ implies that integration over α must be restricted to the interval $[0,\pi/4]$. Note, however, that Eqs. (35) and (36) are inappropriate for numerical evaluation purposes as they introduce a lot of irrelevant crossed terms of vanishing value.

C. Approximation

It appears then from Eqs. (29), (31), and (34) that a complete description of single ionization with excitation to the level n can be obtained from the reduced wave function $\Phi_{nlm}^i(R_n;\Omega)$. In principle, the computation of the latter should involve three steps: (i) interpolation of $\Psi(R,\alpha;\Omega_1,\Omega_2)$ on a two-dimensional $r_1\times r_2$ grid to get $\Psi(r_1,r_2;\Omega_1,\Omega_2)$, (ii) projection onto the hydrogenic state $n\ell m$ of electron i, which implies integration over r_i at fixed $r_{\bar{i}}$, to get $\Psi_{n\ell m}^i(r_1,r_2;\Omega_1,\Omega_2)$, and (iii) interpolation of $\Psi_{n\ell m}^i(r_1,r_2;\Omega_1,\Omega_2)$ on the one-dimensional α grid at $R=R_n$ to get $\Psi_{n\ell m}^i(R_n,\alpha;\Omega_1,\Omega_2)$ and hence $\Phi_{n\ell m}^i(R_n;\Omega)$.

This heavy task would be much alleviated if integration over r_i at fixed r_i^- could be approximated by integration over α at fixed R. The useful range of integration being given by the range r_n of the hydrogenic state n, this will be the case at distances R_n such that the arc $\alpha_n=\tan^{-1}(r_n/R_n)$ can be assimilated to its tangent. This can be done to a good approximation if $\alpha_n \leqslant \Delta\alpha$, where $\Delta\alpha \simeq 10^{-2}$ rad will be referred to as the *allowed angular sector* in the following (see Fig. 3). If the resulting condition $R_n \geqslant 10^2 r_n$ is met, the three steps outlined above reduce to a single one, which consists in letting the projector $P^i_{n\ell m}$ act at fixed $R=R_n$. In this case, the cross section and asymmetry parameter σ_n and β_n can be expressed simply in terms of the integrals

$$I^{\pm}_{n\ell L}(R_n) = \frac{1}{\sqrt{2}} \int_0^{\pi/2} d\alpha \sin\alpha F_{n\ell}(R_n \sin\alpha) \times [a^+_L(R_n;\alpha) \pm a^-_L(R_n;\alpha)], \tag{37}$$

involving the expansion coefficients (8) of the propagated wave function and the hydrogenic radial orbitals (28). One gets

$$\sigma_n = 2\frac{2\pi\omega}{c} R^3 \left(\sum_{\ell=0}^{n-2} |I^+_{n\ell+1\ell}(R)|^2 + \sum_{\ell=0}^{n-1} |I^-_{n\ell\ell}(R)|^2 \right) \tag{38}$$

and

$$\beta_n = \frac{\displaystyle\sum_{\ell=0}^{n-3} \frac{\ell+1}{2\ell+5} |I^+_{n\ell+2\ell+1}(R)|^2 - 6\sum_{\ell=0}^{n-2} \frac{\sqrt{(\ell+1)(\ell+2)}}{2\ell+3} \mathrm{Re}(I^+_{n\ell+1\ell} I^{-*}_{n\ell+1\ell+1}) + \sum_{\ell=0}^{n-1} \frac{\ell+2}{2\ell+1} |I^-_{n\ell\ell}(R)|^2}{\displaystyle\sum_{\ell=0}^{n-2} |I^+_{n\ell+1\ell}(R)|^2 + \sum_{\ell=0}^{n-1} |I^-_{n\ell\ell}(R)|^2}. \tag{39}$$

The fully correlated limit of β_n is obtained as $E \to 0$ and $n \to \infty$, when single ionization with excitation to the level n merges into threshold double ionization. Then, symmetric components and high ℓ values prevail, so that $|I^+_{n\ell+2\ell+1}|^2 \simeq |I^-_{n\ell\ell}|^2 \simeq |I^+_{n\ell+1\ell}|^2 \simeq \mathrm{Re}(I^+_{n\ell+1\ell} I^{-*}_{n\ell+1\ell+1})$ in Eq. (39), and β_n approaches -1, as expected. The opposite uncorrelated limit is obtained for $n=1$, when ionization occurs without excitation. The summations in Eq. (39) reduce then to the only term $\ell=0$ and one gets $\beta_1=+2$ as required.

The above analysis suggests extracting all ionization-excitation data at the largest possible hyper-radius R_{max} since the latter will satisfy $R_{max} \geqslant 10^2 r_n$ for the largest possible set of hydrogenic levels n. This procedure, however, would fail for reasons which show clearly on closer inspection of Fig. 3. At $R_{n<}$, the nth hydrogenic state does not fit the $\Delta\alpha=10^{-2}$ rad allowed angular sector: accordingly, Eqs. (38) and (39) produce spoiled values at this distance. At R_n, the nth hydrogenic state fits the allowed angular sector and its description benefits from the contribution of all α-grid points contained within this sector: the results of Eqs. (38) and (39) should therefore attain their best precision. At $R_{n>}$, the description of the hydrogenic state n deteriorates as the number of α-grid points that span its range decreases. This qualitative analysis prepares one to observe a complex behavior of σ_n and β_n as a function of R. We will see in the next section that the results meet our expectations.

IV. RESULTS

A. Numerical workload

Before presenting the results, it is worth giving an idea of the associated numerical workload, which can be appreciated from a few parameters. Those related to the inner-region calculation are N_ℓ, the number of partial waves in the expansion of the photoionization wave function over bipolar harmonics; N_α, the number of α basis functions; N_R, the number of points in the Lagrange-Jacobi mesh representation of the hyper-radius R; and R_0, the hyper-radius of the inner region. Their role was discussed in [5] and previous publications. The values needed to converge the present very-low-energy calculation of ionization-excitation cross sections are $N_\ell=5$, $N_\alpha=29$, $N_R=90$, and $R_0=60$ a.u. The parameters relevant to the outer-region calculation are n_ℓ, the number of partial waves included in expansion (8); n_α, the number of points in the variable-step-size α grid (17); $d\tau$, the elementary mock time step; and R_{max}, the end point of the hyper-radial propagation. As the cumulated effect of the bielectronic interaction in the course of the propagation is to populate higher and higher partial waves, one has to allow their number to increase substantially in passing from the inner to the outer region. In addition, our goal being to extract ionization-excitation cross sections up to the level $n=50$, taking $n_\ell=50$ guarantees that no contribution to these cross sections will be discarded arbitrarily. We have thus retained this very high value of n_ℓ for the sake of simplicity. We have noted in previous publications that the larger R, the higher the requirements on the description of the regions around $\alpha=0$ and $\pi/2$. Here, the need to achieve accurate projections of the photoionization wave function on ionization-excitation channels which are strongly localized at the edges of the α interval makes these requirements still more severe. They are met, however, by the cubic grid defined by Eq. (17) with $n_\alpha=4000$. Note indeed that for this working grid, the variable α step reaches a minimum of about 0.16×10^{-9} rad at $\alpha=0$ and $\pi/2$, and a maximum of the order

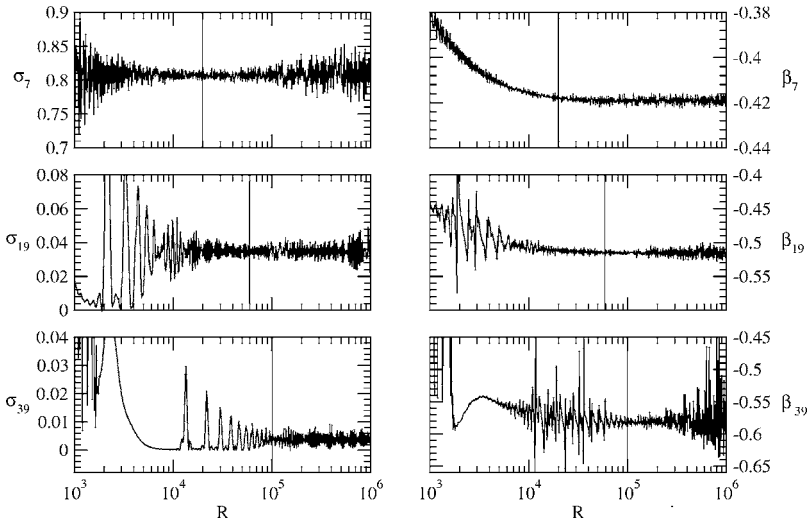

FIG. 4. Calculated cross sections σ_n (in kb) and asymmetry parameters β_n versus R (in a.u.) for $n=7$, 19, and 39. The vertical dashed lines locate the hyper-radial range where physical data can be extracted.

of 0.78×10^{-3} rad at $\alpha=\pi/4$. The elementary constant time step is taken to be $d\tau=0.001$ a.u., which corresponds to a variable R step ranging from 0.025 a.u. at $R_0=60$ a.u. to 86 a.u. at $R_{max}=10^6$ a.u.—for the current energy $E=0.1$ eV. Finally, $R_{max}=10^6$ a.u. proves enough to converge the cross sections of the various processes of interest.

B. Behavior of the cross sections with *R*

Figure 4 illustrates the behavior of the cross section and asymmetry parameter as a function of R for selected levels n. In all cases, two rather chaotic zones at small and large R, respectively, are separated by a large (note the logarithmic scale) and flat plateau which moves toward large R as n increases. This is consistent with our expectations based on the analysis of Fig. 3. To extract the relevant physical information, we compute for each R the running averages $\overline{\sigma_n(R)}, \overline{\beta_n(R)}$ and the corresponding standard deviations $\Delta\sigma_n(R), \Delta\beta_n(R)$ over a hyper-radial interval $R\pm\Delta R$ including 100 neighboring values of R (in a subset of the radial propagation grid comprising one value of R in 100). We then take $\sigma_n=\overline{\sigma_n}(R_n^\sigma)$ and $\beta_n=\overline{\beta_n}(R_n^\beta)$, where R_n^σ and R_n^β minimize the standard deviations $\Delta\sigma_n(R)$ and $\Delta\overline{\beta_n}(R)$, respectively. The associated uncertainties are $\Delta\sigma_n=\overline{\Delta\sigma_n}(R_n^\sigma\pm\Delta R_n^\sigma)$ and $\Delta\beta_n=\overline{\Delta\beta_n}(R_n^\beta\pm\Delta R_n^\beta)$, where ΔR_n^σ and ΔR_n^β define the edges of the R interval corresponding to the above-mentioned plateau. So, in principle, either we may choose the uncertainties—with some arbitrariness—thus defining the plateau unambiguously, or alternatively, we may choose the plateau, thus fixing the uncertainties. However, common sense puts constraints on the relevant R intervals. Clearly, for any value of n, $R_n^\sigma\pm\Delta R_n^\sigma$ and $R_n^\beta\pm\Delta R_n^\beta$ must have a large overlap so that a reasonable ionization-excitation wave function Ψ_n, yielding reasonable integrated *and* differential cross sections, could be extracted within a reasonably large interval $R_n\pm\Delta R_n$. In addition, the evolution of this latter interval with n must be smooth enough. Accordingly, we have chosen our uncertainties to be as small as possible while complying with the above requirements regarding the resulting hyper-radial intervals. The latter are shown on Fig. 5. Their evolution with n mimics that of the quotient $r_n/\Delta\alpha$ of the range of the nth hydrogenic orbital by the allowed angular sector as anticipated in Sec. III C.

C. Ionization-excitation cross sections and asymmetry parameters

The values of σ_n and β_n extracted at the appropriate radii R_n are listed on Table I for $n=4-50$. The cross sections and asymmetry parameters for $n=1-3$, derived from the adiabatic channels defined at R_0, have been added for completeness.

The cross section for single ionization without excitation is 5% (30 kb) higher than the reference value given in [11]. This results from the very localized character of the $1s$ orbital which is not perfectly well accounted for by the present inner-region basis of dimension $N_\alpha=29$. By contrast, the cross section σ_2 is in good agreement with the value of

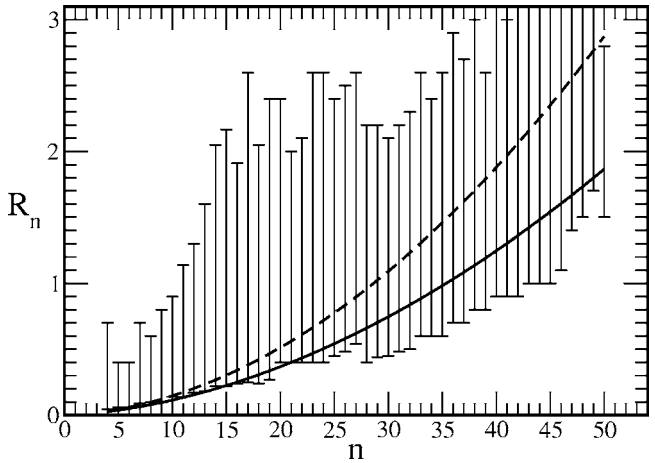

FIG. 5. Hyper-radial range $R_n\pm\Delta R_n$ for the extraction of relevant ionization-excitation data for $n=4-50$. Error bars, $R_n\pm\Delta R_n$ (in 10^5 a.u.); continuous line, $10^2\times$ range of $F_{n\,n-1}(r)$; dashed line, $10^2\times$ range of $F_{n\,0}(r)$. (The range of a radial orbital is defined here as the largest radius where the orbital amplitude is reduced to 1% of its maximum.)

TABLE I. Ionization-excitation cross sections and asymmetry parameters. Estimated uncertainties are given within parentheses in units of the last digit.

n	$\sigma_n \pm \Delta\sigma_n$ (kb)	$\beta_n \pm \Delta\beta_n$	n	$\sigma_n \pm \Delta\sigma_n$ (kb)	$\beta_n \pm \Delta\beta_n$	n	$\sigma_n \pm \Delta\sigma_n$ (kb)	$\beta_n \pm \Delta\beta_n$
1	681	2	18	0.0410(38)	−0.508(3)	35	0.0053(26)	−0.575(7)
2	55	0.86	19	0.0350(36)	−0.515(3)	36	0.0049(24)	−0.58(1)
3	13.75	0.14	20	0.030(3)	−0.523(3)	37	0.0045(24)	−0.58(1)
4	1.834(5)	−0.296(2)	21	0.026(3)	−0.529(3)	38	0.00405(220)	−0.58(1)
5	2.324(5)	−0.344(2)	22	0.022(3)	−0.534(3)	39	0.0038(22)	−0.58(1)
6	1.024(5)	−0.354(2)	23	0.0195(30)	−0.539(5)	40	0.0035(22)	−0.58(2)
7	0.8075(50)	−0.418(2)	24	0.0168(30)	−0.544(5)	41	0.0032(20)	−0.58(2)
8	0.625(5)	−0.399(2)	25	0.015(3)	−0.548(5)	42	0.003(2)	−0.58(2)
9	0.351(5)	−0.456(2)	26	0.0132(30)	−0.552(5)	43	0.0028(18)	−0.58(2)
10	0.240(4)	−0.464(2)	27	0.0120(28)	−0.556(5)	44	0.0026(18)	−0.59(2)
11	0.184(4)	−0.455(2)	28	0.0104(28)	−0.559(5)	45	0.0024(18)	−0.59(2)
12	0.145(4)	−0.456(2)	29	0.0093(28)	−0.562(5)	46	0.0023(18)	−0.59(2)
13	0.114(4)	−0.463(2)	30	0.0084(28)	−0.564(5)	47	0.00215(160)	−0.59(2)
14	0.090(4)	−0.472(2)	31	0.0080(28)	−0.567(5)	48	0.0020(14)	−0.59(2)
15	0.072(4)	−0.485(2)	32	0.0070(26)	−0.569(7)	49	0.0018(14)	−0.59(2)
16	0.0600(38)	−0.493(2)	33	0.0063(26)	−0.571(7)	50	0.0018(14)	−0.59(2)
17	0.0500(38)	−0.500(3)	34	0.0058(26)	−0.573(7)			

57 ± 3 kb that can be inferred from the same reference. The cross section $\sigma_3 = 13.75$ kb is again overestimated with respect to the recommended value of the order of 11 kb. But this inaccuracy has nothing to do with the finite dimension of the α basis in the inner region. Indeed, it indicates that the level $n=3$ does not fully decouple adiabatically from the rest of the wave function at $R_0 = 60$ a.u. The results obtained for $n=4$ should therefore be taken with caution since part of the flux that should go into this level is inappropriately suppressed by the truncating of the wave function at R_0. This slight inaccuracy inherent in the adiabatic truncating at R_0, however, does not affect the results obtained for higher levels. Regarding the asymmetry parameter, $\beta = 2$ is obtained for $n=1$ as required, but nothing more can be said, as no results are available for comparison at this very low energy.

From $n \geqslant 10$ (12), we observe a smooth monotonic decay of σ_n (β_n) with n, as shown by Figs. 6 and 7. This behavior reflects the increasingly correlated character of the ionization-excitation process to increasingly high levels n: namely, low β_n implies strong electron-electron correlations, while low σ_n evidences how difficult it is to maintain strong correlations over the very large spatial range of highly excited levels n. Note that our previously published values of σ_n for $n = 10-24$ [9] cannot be distinguished from the present ones at the scale of the figure.

It is difficult to find relevant material for comparison with the present calculations. To our knowledge, no previous data have ever been obtained regarding ionization excitation to levels beyond $n=10$. Moreover, previous work regarding the partial ionization cross sections and asymmetry parameters for excitation to the levels $n \leqslant 10$ has focused on photon energies different from the present 79.1 eV. A large number of these studies including recent ones [12–14] are motivated by the interest in the doubly excited states of helium. The photon energies considered therefore span a region where the strong effects of resonances preclude any comparison with above-the-double-ionization-threshold data. More relevant to our present purpose is a series of HSCC [15], eigenchannel $\mathcal{R}$-matrix [16], and CCC [17] calculations of the ratio $\rho_n = \sigma_n^+ / \sigma_1^+$ for $n = 2-4$, 2–6, and 2–6, respectively, in the 80 eV–1 keV photon energy range. These theoretical predictions are in excellent agreement with each other and with the available experimental results [18] above 100 eV. Despite a slight deterioration of their agreement at lower photon energy, these data can nevertheless be tentatively extrapolated down to the double-ionization threshold, yielding values of about 8.5%, 1.75%, 0.65%, 0.25%, and 0.1% for ρ_n, $n = 2-6$, respectively. These estimates can be compared with our calculations at 79.1 eV photon energy yielding 8.1%,

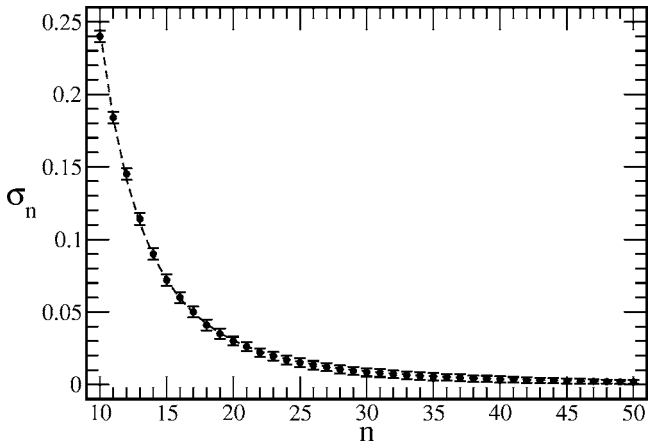

FIG. 6. Ionization-excitation cross sections from $n = 10-50$. Full circles with error bars, calculated values of σ_n (in kb); dashed line, best n^{-3} fit (see text).

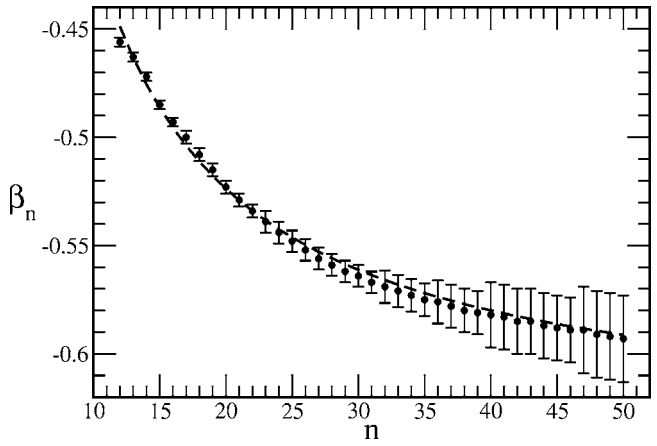

FIG. 7. Ionization-excitation asymmetry parameters from $n=12$ to 50. Full circles with error bars, calculated values of β_n; dashed line, best fit (see text).

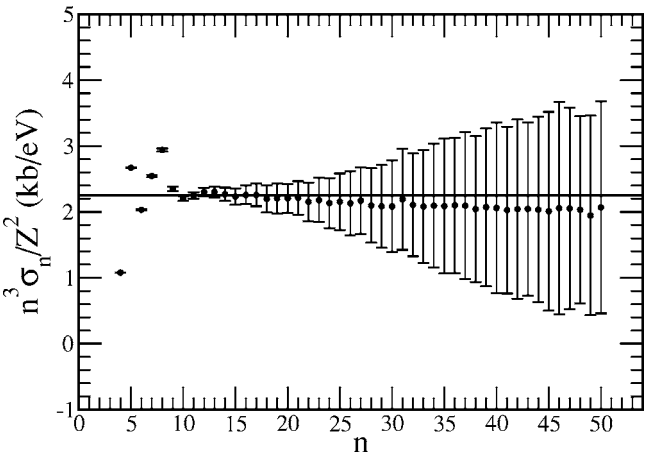

FIG. 8. Extrapolating the ionization-excitation cross sections to infinite n. Dots with error bars, calculated values of $n^3\sigma_n/Z^2$ (kb/eV); horizontal line, best constant fit (see text).

2%, 0.27%, 0.34%, and 0.15%. The two sets of data are roughly compatible, it being understood that our value of ρ_4 has to be taken with caution as explained previously. Similarly, the β_2 parameter reported in [15] can be extrapolated to a value of 0.8 at threshold, consistent with our calculated value of 0.86 at 0.1 eV above this threshold.

Comparisons can also be made, at least qualitatively, between our data and the results of threshold photoelectron measurements performed in resonance-free energy ranges [19–21]. Focusing on the highest levels available, we note that the cross sections $\sigma_8=0.77(7)$, $\sigma_9=0.43(7)$, and $\sigma_{10}=0.37(6)$, recorded at the respective thresholds of 78.12, 78.30, and 78.46 eV [19] seem consistent with our 79.1 eV values of 0.625(5), 0.351(5), and 0.240(4) kb. As to the β_5 and β_6 parameters reported in the same and a subsequent study [20], they do not exhibit the expected decay with increasing n and decreasing energy, so that we prefer to discard them from the present discussion. By contrast, the asymmetry parameter β_{10} measured at 78.11 eV photon energy, which amounts to 0.25 eV above the threshold [21], takes the value −0.48 which appears to be consistent with our result of −0.464 at 79.1 eV.

On the other hand, definite predictions have been formulated regarding the limit of the partial ionization cross sections as $n\to\infty$ at fixed energy E. It is indeed widely accepted [18,22,23] that in this limit, the ionization-excitation cross section per unit energy range in the quasicontinuum formed by highly excited states of the residual ion tends toward the energy-differential cross section for double ionization under fully asymmetric energy sharing. This can be written

$$\lim_{n\to\infty}\left(\frac{dn}{dE_n}\sigma_n(E)\right)=\frac{d\sigma^{2+}}{dE_1}(E,E_1=E). \tag{40}$$

As the arguments behind (40) concern the ionization-excitation process as a whole it is tempting to theorize that

$$\lim_{n\to\infty}\beta_n(E)=\beta^{2+}(E,E_1=E). \tag{41}$$

Then, one advantage of having such an extended set of partial ionization cross sections and asymmetry parameters as the one available here is that one can attempt extrapolating to infinite values of n in order to check the above conjectures.

Extrapolation, however, is a delicate task that can be performed with full confidence only if the functional dependence of the dependent variable on the independent variable is known for sure. This turns out to be the case, at least to some extent, for σ_n. As $dE_n/dn=Z^2/n^3$, Eq. (40) indeed implies that σ_n behaves as n^{-3} for large n. However, no precise indication is available as regards the values of n beyond which this behavior sets in. To get an idea of this value, we have plotted $n^3\sigma_n/Z^2$ for n ranging from 4 to 50. Figure 8 evidences a stabilization of this product at about 2.2 kb/eV from $n=10$ to 20, followed by a steady decay leading to a value of 2 kb/eV at $n=50$. However, it is possible to draw a horizontal line at 2.2 kb/eV through the error bars from $n=10$ to 50—the latter being magnified by the same factor n^3/Z^2 as the cross sections for consistency. We can thus state that our data are consistent with the n^{-3} law setting in from $n=10$. Accordingly, we have fitted the expression Z^2C/n^3 to the cross-section data in Fig. 6, obtaining an excellent fit for $C=2.25$ kb/eV in agreement with what we could infer from Fig. 8.

The case of the asymmetry parameter is more difficult as the rate of its evolution toward an n-independent constant at $n=\infty$ is unknown. To get an idea of this rate, we have fitted expressions of the form $C(1+C'/n^p)$ to our data in Fig. 7 for $p=0.5,1,1.5$. A significantly better fit is obtained for $p=1$, yielding a tentative value $C=-0.636$ for the limit of interest, which lies still far from the −1 value predicted at threshold in [24]. The forthcoming study of double ionization at the same very low excess energy of 0.1 eV will shed more light on this apparent contradiction.

V. CONCLUSION

We have presented a fixed-R projection technique which allows the H$\mathcal{R}$MSOW method to provide ionization-excitation cross sections and asymmetry parameters. Thanks to this extension, this method now supplies a comprehensive

description of the dynamics of the helium atom above its full fragmentation threshold. We have chosen to illustrate its capabilities in the near-threshold region which is characterized by a strong competition between the infinite set of open channels including single ionization, single ionization with excitation, and double ionization. Ionization-excitation cross sections and asymmetry parameters at 0.1 eV above the double-ionization threshold are presented here for levels up to $n=50$, and tentative asymptotic limits n_∞ and β_∞ are proposed. A forthcoming study will present the complementary double-ionization data and discuss the relation between ionization-excitation to very weakly bound states and double ionization in detail. It will thus complete the demonstration that the H$\mathcal{R}$MSOW method provides control of the three-body Coulomb dynamics at very low energy. This property will be exploited in future work: we consider revisiting the Wannier threshold law as well as moving below the double-ionization threshold to explore the region of high-lying doubly excited states.

ACKNOWLEDGMENT

The authors acknowledge the support of the CNRS computer center IDRIS (Orsay, France) through the Project No. 041485.

[1] J. S. Briggs and V. Schmidt, J. Phys. B **33**, R1 (2000).
[2] L. Malegat, in Proceedings of the XXIII ICPEAC [Phys. Scr., T 110, 83 (2004)].
[3] L. Malegat, P. Selles, and A. K. Kazansky, Phys. Rev. Lett. **85**, 4450 (2000).
[4] P. Selles, L. Malegat, and A. K. Kazansky, Phys. Rev. A **65**, 032711 (2002).
[5] P. Selles, L. Malegat, A. Huetz, A. K. Kazansky, S. A. Collins, D. P. Seccombe, and T. J. Reddish, Phys. Rev. A **69**, 052707 (2004).
[6] L. Malegat, P. Selles, and A. K. Kazansky, in *Many Particle Quantum Dynamics in Atomic and Molecular Fragmentation*, edited by V. P. Shevelko and J. Ullrich (Springer-Verlag, Heidelberg, 2003).
[7] M. D. Feit, J. A. Fleck, Jr., and A. Steiger, J. Comput. Phys. **47**, 412 (1982).
[8] R. W. Hockney and C. R. Jesshope, *Parallel Computers: Architecture, Programming, and Algorithms* (Adam Hilger, Bristol, 1981).
[9] P. Selles, L. Malegat, and A. K. Kazansky, in *Electron and Photon Impact Ionization and Related Topics 2004*, edited by B. Piraux, IOP Conf. Ser. No. 183 (Institute of Physics, London, 2005), p. 141.
[10] *Handbook of Mathematical Functions*, edited by M. Abramowitz and I. Stegun (Dover, New York, 1972).
[11] J. M. Bizau and F. J. Wuileumier, J. Electron Spectrosc. Relat. Phenom. **71**, 205 (1995).
[12] T. Schneider, Chien-Nan Liu, and J. M. Rost, Phys. Rev. A **65**, 042715 (2002).
[13] H. W. van der Hart and C. H. Greene, Phys. Rev. A **66**, 022710 (2002).
[14] Y. H. Jiang, R. Püttner, R. Hentges, J. Viefhaus, M. Poiguine, U. Becker, J. M. Rost, and G. Kaindl, Phys. Rev. A **69**, 042706 (2004).
[15] J. Z. Tang and J. Burgdörfer, J. Phys. B **30**, L523 (1997).
[16] K. W. Meyer, J. L. Bohn, C. H. Greene, and B. D. Esry, J. Phys. B **30**, L641 (1997).
[17] A. S. Kheifets and I. Bray, Phys. Rev. A **57**, 2590 (1998).
[18] R. Wehlitz, I. A. Sellin, O. Hemmers, S. B. Whitfield, P. Glans, H. Wang, D. W. Lindle, B. Langer, N. Berrah, J. Viefhaus, and U. Becker, J. Phys. B **30**, L51 (1997).
[19] P. A. Heimann, U. Becker, H. G. Kerkhoff, B. Langer, D. Szostak, R. Wehlitz, D. W. Lindle, T. A. Ferrett, and D. A. Shirley, Phys. Rev. A **34**, 3782 (1986).
[20] D. W. Lindle, P. A. Heimann, T. A. Ferrett, and D. A. Shirley, Phys. Rev. A **35**, 1128 (1987).
[21] R. I. Hall, L. Avaldi, G. Dawber, M. Zubek, K. Ellis, and G. King, J. Phys. B **24**, 115 (1991).
[22] S. Svensson, A. Kikas, A. Ausmees, S. J. Osborne, S. Aksela, A. Naves de Brito, and E. Nõmmiste, J. Phys. B **28**, L293 (1995).
[23] R. Wehlitz, M.-T. Huang, I. A. Sellin, and Y. Azuma, J. Phys. B **32**, L635 (1999).
[24] C. H. Greene, J. Phys. B **20**, L357 (1987).
[25] T. Suric and R. H.Pratt,J. Phys. B **37**, L93 (2004).